Design and Development of Small-Scale Autonomous Vehicles for High-Speed Racing

Israel Charles, Owen Burns, Casey Jack, Tevin Mukudi, Asa Daboh
College of Engineering and Computer Science
University of Central Florida
Orlando, USA
Israel.Charles@ucf.edu, Owen.Burns@ucf.edu, Casey.Jack@ucf.edu, te052960@ucf.edu, Asa.Daboh@ucf.edu

***Abstract*—This paper presents the design of two small-scale autonomous racing vehicles to serve as a low-cost platform for testing and research in self-driving technologies. The proposed system integrates a reinforced Traxxas Slash 4x4 chassis for robustness and modularity, a Power Management and Distribution System (PMS) to ensure safe and efficient voltage regulation, and a high-performance computing unit (Jetson Xavier NX) for real-time AI-capable based perception and control. A belt-driven drivetrain upgrade, along with precise weight balancing and adjustable suspension, improves vehicle handling and acceleration. The software architecture, built on ROS 2 Foxy, leverages the SLAM Toolbox and Nav2 frameworks for mapping, localization, and motion planning. Two control stages, exploration and race line follow, enable dynamic environment mapping and optimal path execution, while a dedicated Status Indicator Subsystem delivers essential telemetry and diagnostics to operators via a touchscreen interface. Experimental results confirm the viability of this approach, providing a compact, stable, and extensible racing platform for advanced autonomy research.**

Index Terms—Autonomous Racing, Small-Scale Vehicles, ROS 2, SLAM, Power Management, Sensor Fusion, Status Indicator.

I. Introduction

In today's world, autonomous navigation is rapidly evolving, with self-driving cars promising to reshape the transportation landscape. However, developing and testing such technologies on full-sized vehicles can be expensive and time-consuming. As a result, researchers have turned to smaller-scale racing vehicles to safely and cost-effectively evaluate new ideas. These miniature platforms provide a robust testing environment for computer vision, real-time decision-making, and advanced control systems, capabilities that are directly transferable to larger, real-world applications.

One notable advocate for autonomous vehicle research using small-scale vehicles is the RoboRacer Foundation [1], previously known as F1Tenth. It was established to promote education and research in autonomous driving by organizing competitions for small-scale electric vehicles. These small-scale vehicles help researchers and students validate new concepts safely by avoiding large-scale risks by testing in a controlled environment. It helps to save costs by using smaller platforms, lowering initial investment in hardware and resources. It accelerates development cycles since now rapid prototyping is easier, with vehicles, parts, and sensors being more accessible and interchangeable.

By bridging theoretical developments in autonomous navigation with hands-on implementations, this project aims to make tangible contributions to the future of self-driving cars and intelligent transportation systems.

A. Goals & Objectives

The long-term vision of this project is to establish a sustainable RoboRacer team at the University of Central Florida (UCF), ensuring that future cohorts of students have a platform to explore and advance autonomous vehicle technologies. A near-future application of our work is to compete in the 2025 RoboRacer Grand Prix at ICRA [2], where we will showcase our two autonomous race vehicles: one adhering to the hardware limitations of the closed class and the other featuring performance enhancements allowed under the rules of the open class. To achieve competitive performance, both vehicles must successfully navigate previously unseen racetracks without crashing and the shortest possible lap times. Key engineering specifications have been defined to guide the design and development process, as summarized in Table I.

TABLE I
KEY ENGINEERING SPECIFICATIONS

Item	Parameter	Specification
Assembled Vehicles	Weight distribution	50/50 (±10%)
	0–14.5 mph time diff (open vs closed class)	>5% decrease
Control Algorithm	Replanning time	avg <0.5 sec
	Race line computation time	avg <10 sec
Power Board	Efficiency	>60%

These targets ensure that the vehicles effectively balance both mechanical and computational requirements. Each assembled vehicle must maintain a static weight distribution of 50/50, with an allowable margin of ±10%. The reinforced vehicle is required to achieve at least a 5% reduction in 0–14.5 mph acceleration time compared to the stock mechanical design. The power distribution board should operate at an efficiency greater than 60% to preserve battery life, while the control algorithm must be capable of replanning in under <0.5 s to adapt to dynamic track conditions. Meeting these

This project was funded by the lab CAVREL under the supervision of Dr. Yaser Fallah

objectives validates that the resulting platforms are robust enough for high-speed autonomous racing.

II. System Architecture Overview

This section provides an overview of the vehicles' system architecture, highlighting the key hardware and control components and their interconnections. Fig. 1 presents a high-level block diagram that illustrates how power and data flow among the various subsystems. Each subsystem plays a critical role in ensuring that the vehicle can deliver high performance in a small-scale racing environment, from efficient power distribution and real-time data processing to robust sensing and precise control.

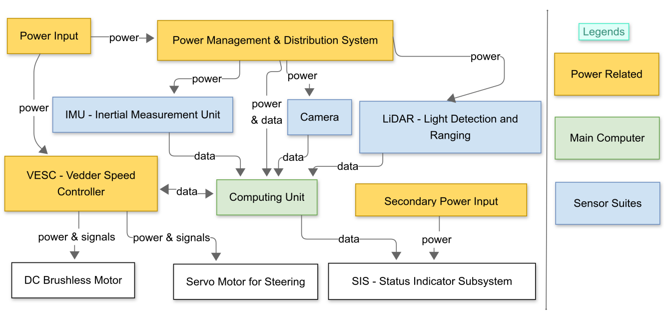

Fig. 1. Small-Scale Autonomous Racing Vehicles Block Diagram.

A. Overall System Layout

As shown in Fig. 1, the Power Input (3S Lipo Battery in our case) supplies electrical energy to the Power Management & Distribution System (PMS) and the VESC (Vedder Electronic Speed Controller). The PMS, in turn, provides regulated power to the LiDAR, Camera, IMU, and Computing Unit (CU). Meanwhile, the VESC drives the DC Brushless Motor and the Servo Motor (for steering) and interfaces with the CU for data exchange. The CU processes sensor data from LiDAR, Camera, and IMU, then sends control commands back to the VESC and communicates system health and performance data to the Status Indicator Subsystem (SIS). Finally, a secondary power input (battery) also supplies power directly to the SIS since that subsystem is separated from the main vehicle.

B. Mechanical Chassis

All subsystems are mounted on the Traxxas Slash 4x4 Ultimate chassis. This chassis was selected for its robust construction and ample space, which allow the integration of sensors, computing hardware, and a high-capacity battery. Key features include a dimension of 22.4 × 11.7 × 7.6 inches (L × W × H) with a ground clearance of 2.8 inches. It weighs approximately 2.9 kg (without added components). It has fully independent four-wheel drive (4WD) with adjustable suspension and torque control. The motor is a Velineon 3500 brushless motor powered by a 5000 mAh 11.1 V 3S LiPo battery. This chassis is known for its durability, waterproof electronics, high-quality shocks, and rugged suspension.

These features ensure the platform remains stable and can accommodate both the computational load and the added weight of additional sensors.

C. Power Management & Distribution System (PMS)

At the core of the vehicle's electrical design is the Power Management & Distribution System (PMS). Power from the battery flows to the PMS, which regulates voltage levels, routes power, and protects components from electrical surges. By splitting and conditioning power for different subsystems, especially the sensitive sensors and computing unit, the PMS ensures consistent performance and prevents damage from power fluctuations. This arrangement is crucial for reliable, continuous operation at high speeds.

D. Computing Unit (CU)

The Computing Unit acts as the "brain" of the vehicle, handling the perception, planning, and control tasks essential for autonomous racing. This project utilizes the Jetson Xavier NX, chosen for its high Computational Power (6-core Carmel ARM v8.2 64-bit CPU) and 384-core Volta GPU with 48 Tensor Cores for real-time AI processing. The unit has a memory of 8 GB of LPDDR4x, capable of smoothly managing the perception and control algorithms simultaneously. Its compact form factor makes it easy to mount on the vehicle chassis while leaving ample space for sensors and other peripherals. It also has built-in Wi-Fi for remote access via SSH, enabling streamlined development and testing. Because the vehicle navigates unknown racetracks, real-time vision and control algorithms must run efficiently to enable split-second decision-making. The CU's ability to process large volumes of sensor data and produce actuator commands quickly is critical for competitive racing performance.

E. Motor Control

Driving a brushless motor for a high-speed racing application requires a motor controller that provides both fine control and comprehensive telemetry. This project employs a Trampa VESC 6 MKVI, selected for its advanced control capabilities, essential for handling dynamic racing conditions. It can provide real-time data feedback to the CU, facilitating closed-loop control and performance monitoring. In addition to that, it has an Integrated Inertial Measurement Unit (IMU) that can supply angular rate and acceleration data, reducing the need for additional external IMU hardware. By consolidating motor control and inertial sensing in a single unit, wiring complexity is minimized, and state-estimation accuracy improves, both of which are critical for high-speed maneuvers.

F. Perception Sensor Suites

The system relies on multiple sensors to detect obstacles, gauge distances, and track vehicle orientation:

1) LiDAR (Hokuyo UST-10LX): Chosen for its 40 Hz refresh rate, 10-meter range, and 270° field of view. Its compact design and rapid scanning capabilities make it highly effective for detecting obstacles in indoor racing environments with limited space.

2) Camera (Intel RealSense D435i): A stereo/depth camera offering high refresh rates and real-time dense depth data. This camera complements LiDAR by providing a more complete 3D understanding of the environment, enabling robust obstacle detection and navigation.

3) IMU (Integrated with VESC): Accurate inertial measurements are vital for stable control, particularly during high-speed turns and rapid accelerations.

G. System Status Indicator Subsystem (SIS)

The System Status Indicator Subsystem (SIS) serves as a real-time "dashboard," providing vital feedback on the vehicle's performance, power levels, and overall health. This module ensures rapid diagnostics and status reporting, critical for operators during testing and racing. Since it is a handheld device, it draws power from its own power input source (batteries).

III. Mechanical Design AND Optimization

In order to maximize performance, both the closed-class and open-class vehicles underwent mechanical modifications focused on the drivetrain, weight distribution, and suspension. While the closed-class vehicle was constrained mainly to suspension tuning and weight distribution, the open-class vehicle was further optimized through component replacements and additional design enhancements. The details of these modifications are presented in the subsections below.

A. Drivetrain

Achieving strong acceleration is critical for competitive lap times [3]. Accordingly, the open-class vehicle's goal was to reduce the 0–14.5 mph time by at least 5% and attain a power-to-weight ratio above 126.6 W/kg. After considering various approaches, we replaced the stock motor with a more powerful one. We opted for the KingVal 3650 (4300 Kv), rated at 900 W, which exceeded the original motor's 721.6 W rating by more than 10%. Under ideal conditions (constant mass, negligible losses, and no aerodynamic drag), increased motor power translates directly into higher torque and, thus, greater linear acceleration. This direct proportional relation is deduced from the power equation (1) and linear acceleration equation (2) as follows:

$$P = \tau \cdot \omega, \tag{1}$$

$$a = \frac{\tau \cdot R}{r \cdot m}, \tag{2}$$

where P is power, τ is torque, ω is angular velocity, R is the gear ratio, r is the wheel radius, and m is vehicle mass. Equation (1) asserts that as power increases over a range of angular velocities, the torque increases. Additionally, (2) asserts that as the torque increases, given a constant gear ratio, wheel radius, and vehicle mass, the linear acceleration also increases. Therefore, under ideal conditions, an 5% increase in the power of the drive motor would result in a 5% increase in the linear acceleration capabilities of the vehicle. In selecting a replacement motor for the vehicle, a factor of safety of 2 was applied to the power increase goal to account for the unideal conditions of the vehicle's operation. By ensuring the new motor has at least 10% more power, we mitigate non-ideal effects such as friction and traction losses.

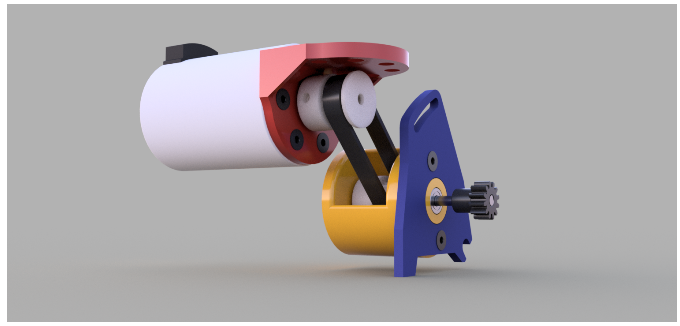

Fig. 2. Fusion 360 render of the belt-drive mechanism.

To integrate the KingVal 3650 motor, we designed a belt-drive system, shown in Fig. 2, that uses timing belts. The belt drive mechanism was designed to minimize slippage, maximize mechanical efficiency, and enable effective load transfer over short distances. Belt slippage leads to energy loss, as it prevents the motor's power from being fully transmitted through the drivetrain. Among the belt types evaluated, the timing belt emerged as the optimal solution. When properly implemented, it completely eliminates slippage. This not only enhances efficiency but also makes it the most effective option for short-distance load transfer. The final design incorporated GT2 pulleys, a 3 mm stainless steel shaft, and 8 mm ball bearings.

Given a 900-watt motor and a weight budget of 5.7 kg, the open class vehicle achieves a power-to-weight ratio of approximately 157.9 W/kg, comfortably exceeding the target of 126.6 W/kg.

B. Weight Distribution

Balanced weight distribution significantly affects vehicle handling. Excessive oversteer or understeer can diminish lap times and increase crash risk [4]. Oversteer occurs when the rear wheels lose traction relative to the front wheels, causing the vehicle to rotate more than intended. This results in a tighter turning radius and can lead to the car spinning out. In contrast, understeer happens when the front wheels lose traction, causing the vehicle to turn less than intended and potentially run wide off the track.

During acceleration, weight shifts toward the rear, increasing rear-wheel traction, while braking shifts weight forward, enhancing front-wheel traction. These dynamic weight shifts can induce oversteer or understeer. If the static weight distribution is imbalanced, these effects can become exaggerated, compromising the vehicle's handling performance. To promote stable and predictable handling, making control easier for the software, the vehicle is designed with a 50/50 weight distribution between the front and rear axles to avoid exacerbating weight-transfer effects during acceleration or braking.

Achieving this distribution involved strategic component placement, as seen in Fig. 3, along the vehicle's centerline. By

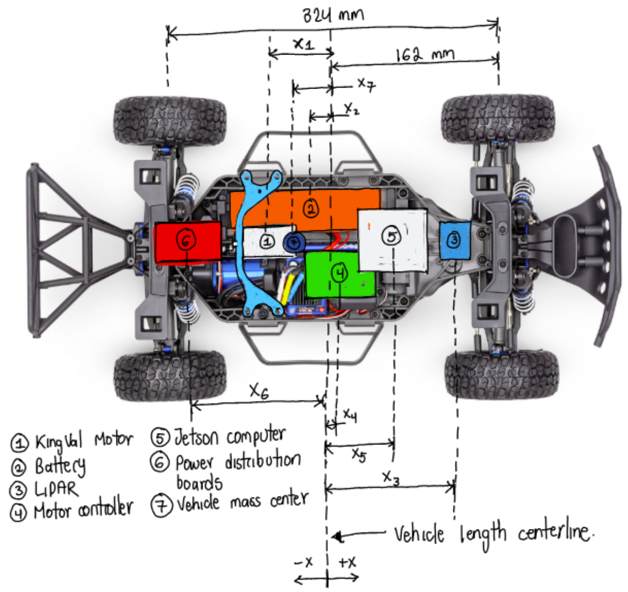

Fig. 3. Placement of major components of the vehicle to achieve 50/50 weight distribution.

adjusting the location of the battery, computing unit, and other modules, the center of mass was brought near the geometric midpoint. Table II summarizes the resulting measurements, indicating that the actual front-to-rear distribution closely matches the ideal 50/50 goal.

TABLE II
WEIGHT DISTRIBUTION TEST DATA

Measurement Point	Goal (g)	Actual (g)	% Difference
Front Axle	1578.45	1432.90	9.2%
Rear Axle	1578.45	1665.80	5.5%

C. Suspension

To achieve a stable racing platform through corners, we prioritized reducing body roll caused by lateral acceleration. Excessive body roll can compromise tire contact with the track, reducing overall grip and increasing the risk of software losing control due to insufficient mechanical traction. Vehicles with minimal body roll maintain better contact across all tires, enhancing stability and control [5].

There are several strategies to reduce body roll, and our objective was to implement a method with an effectiveness greater than 1.25, meaning it would reduce body roll by at least 25% compared to a baseline configuration. Among the techniques studied, lowering the vehicle's center of gravity (CoG) or raising the roll center emerged as the most cost-effective and easily tunable options.

Component placement played a key role in this strategy. By adjusting the vertical positions of components, we were able to manipulate the CG height and, in turn, influence the vehicle's roll behavior. The relationship between roll angle ϕ and CoG-roll center distance is captured by the following equation:

$$\phi = \frac{m\, g\, \Delta h}{C_{\mathrm{Ro},f} + C_{\mathrm{Ro},r}}, \tag{3}$$

where Δh is the distance between the CoG and roll center, m is mass, and g is gravitational acceleration. Equation (3) shows that roll angle is directly proportional to the distance between the center of gravity and the roll center. Therefore, all else being equal, reducing Δh proportionally decreases the roll angle ϕ.

To meet our effectiveness target, the CoG-roll center distance had to be reduced to less than 80% of its initial value. Achieving this theoretically ensures a roll reduction of at least 25%, satisfying the target effectiveness of >1.25, thereby improving overall cornering performance.

IV. POWER MANAGEMENT SYSTEM

The Power Management System (PMS) is responsible for distributing power from on-board batteries to key vehicle subsystems while monitoring input and output levels in real time. Live data are then relayed to the Status Indicator Subsystem for display. The design of the PMS prioritized four key factors: robust *hardware architecture*, adequate *heat dissipation*, appropriate *circuit protections*, and high *efficiency*.

A. Hardware Design and Architecture

Fig. 4 illustrates the fundamental schematic used for the Power Management System (PMS), with red arrows denoting power connections and black arrows representing data connections. The electrical and data flow is as follows: the system can selectively draw power from either Lithium-Polymer (LiPo) batteries or a 19V DC input jack. LiPo batteries were chosen due to their high energy density and lightweight construction. Their voltage levels are continuously monitored by the PMS's onboard microcontroller—an ESP32—to accurately determine the remaining battery capacity.

Given that the ESP32's analog-to-digital converter (ADC) accepts a maximum input of only 3.3V on its GPIO pins, the higher battery voltage must first be stepped down. This is achieved through a simple resistor voltage divider, governed by the equation: Equation (4) governs the voltage step-down:

$$V_2 = V_1 \cdot \frac{R_2}{R_1 + R_2}, \tag{4}$$

In (4), V_1 is ideally 19V, but the design uses 20V to safely account for potential voltage fluctuations. The target output voltage, V_2 is 3.3V suitable for ESP32 input, resulting in calculated resistor values of $R_1 = 10\mathrm{k}\Omega$ and $R_2 = 2\mathrm{k}\Omega$. These resistor values were chosen to ensure minimal power consumption and maintain measurement accuracy for the ADC.

The current flowing through the voltage divider resistors can be determined using:

$$I_r = \frac{V_1}{R_1 + R_2}. \tag{5}$$

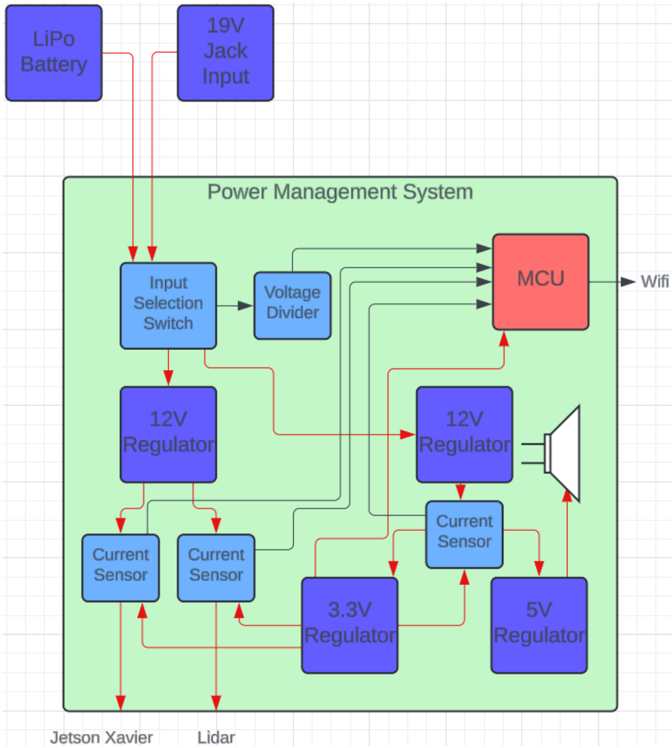

Fig. 4. Power Management System architecture.

According to (5), with an input voltage of approximately 19V, the current draw is roughly $I_r \approx 1.5\,\text{mA}$, and during typical race conditions at about 11V, the current is around $917\,\mu$A, These low currents ensure efficiency while avoiding excessively high resistor values, which could negatively impact ADC accuracy.

After voltage monitoring, the input voltage feeds into two separate 12V voltage regulators. The first 12V regulator provides power directly to the onboard computer (Jetson Xavier NX) and the LiDAR sensor. Each of these components' current consumption is independently monitored using dedicated current sensors that employ shunt resistors. A shunt resistor, specifically a low-value 2mΩ high-power resistor, introduces negligible interference with circuit performance. The current flowing through it can be calculated by measuring the voltage drop across it and dividing by its resistance.

The second 12V regulator, identified as "12Vcc" to distinguish it, powers two additional voltage regulators: a 3.3V regulator and a 5V regulator. The 3.3V regulator exclusively supplies components within the PMS itself, such as the ESP32 microcontroller and four current sensors. The 5V regulator powers the PMS indicator buzzer. Two of the four current sensors were previously mentioned; the remaining two monitor the current drawn by the 12Vcc and the 5V regulators, respectively. All collected current sensor data is relayed to the ESP32 microcontroller through the I^2C communication protocol.

After collecting and processing this information, the ESP32 transmits the data wirelessly via Wi-Fi to a remote indicator subsystem for real-time display. Lastly, the aforementioned buzzer, powered at 5V, is controlled by the ESP32 through a Bipolar Junction Transistor (BJT). Since the ESP32 GPIO pins output a maximum of 3.3V, but the selected buzzer requires a 5V supply for optimal operation, the BJT serves as a necessary interface component.

B. *Heat Dissipation*

Heat dissipation is critical, given the high currents and voltages involved. To mitigate overheating, the PCB layout employs a four-layer design with dedicated copper planes for power distribution. Increasing copper surface area allows heat to spread, lowering the risk of thermal hotspots. Further, the PMS is partitioned into six smaller PCBs (one per regulator, plus an ESP32 board and a motherboard) rather than a single monolithic board. This modular approach adds surface area for heat to dissipate and simplifies maintenance.

C. *Circuit Protections*

For the Power Management System (PMS), several protective measures were implemented to minimize component failure risks. As previously discussed, effective heat dissipation is essential to prevent overheating caused by high current demands. Another critical concern is electrostatic discharge (ESD), also known as transient voltage or static electricity, which occurs when accumulated electric charges, often on a human body, discharge upon contact with the circuit board. Although the physical shock from ESD might feel minor, the underlying voltage can reach thousands of volts, posing a significant risk to sensitive electronic components. To mitigate this threat, transient voltage suppression (TVS) diodes were incorporated to protect the ESP32 microcontroller. TVS diodes feature a high reverse breakdown voltage capability (typically thousands of volts), effectively diverting and suppressing voltage spikes before they reach sensitive electronics.

Similarly, bypass capacitors, also referred to as decoupling capacitors, have been employed as an additional protective measure. Since capacitors inherently block DC and allow AC signals to pass through, placing them immediately after DC voltage regulators and connecting them directly to ground reduces high-frequency noise in the voltage supply. This noise reduction is particularly important in our PMS design because we have opted for highly efficient switching regulators, known for generating considerable high-frequency output noise. Lastly, the PMS incorporates Schottky diodes as part of its protective scheme. Schottky diodes, distinguished by their low forward-voltage drop, are placed in series with the system's power inputs to prevent reverse voltage conditions, ensuring current does not flow backward into the power supply and damage upstream components.

D. *Efficiency*

Although the chosen LiPo batteries offer high capacity, their energy is finite. Our vehicle demands substantial electrical power to achieve high speeds, while simultaneously requiring minimal weight to reduce the load on the electric motors. For this reason, efficiency was a critical design consideration for the Power Management System (PMS). Reducing the PMS's own power consumption allowed us to allocate more energy toward essential vehicle components, influencing our selection of specific components accordingly.

All voltage regulators employed in the PMS are switching-type regulators. These regulators were selected due to their significantly higher efficiency compared to alternative methods, such as simple resistor-based voltage dividers or Low-Dropout (LDO) linear regulators.

To thoroughly evaluate the efficiency of our system, we conducted tests across the full spectrum of conditions that our voltage regulators might encounter. Testing involved varying the input voltage between the minimum and maximum expected operating conditions, as well as adjusting the load (and consequently current draw) at multiple input voltage levels using an electronic load. Our primary focus was on the 12V regulators, as they are the first to receive power input in our system. Specifically, we varied the input voltage from a minimum of 8V to a maximum of 20V. At each voltage step, the load current was adjusted between 100 mA and 400 mA. Although testing with higher current values was desirable, our 12V regulator encountered performance issues beyond approximately 500 mA during preliminary tests, limiting our measurements to 400 mA.

During testing, we monitored critical parameters, including stable output voltage and input current, to verify correct regulator operation. Using these measurements, we calculated input and output power with the equation:

$$P = V \times I, \tag{6}$$

Subsequently, we determined power efficiency using:

$$\text{Eff} = \frac{P_{\text{out}}}{P_{\text{in}}} \times 100\%. \tag{7}$$

The results of our efficiency testing for the 12V regulators under varying input voltage and output current conditions are shown in Fig. 5. As illustrated, the efficiency decreases with increasing load current and decreasing input voltage; however, the efficiency consistently remained above 80% across all tested scenarios.

V. SOFWARE DESIGN & ARCHITECTURE

The control algorithm for this project leverages established self-driving principles, including formal methods for mapping, localization, planning, and control. This approach was chosen over reinforcement learning due to the extensive community support and the high cost associated with training-based methods. As illustrated in Fig. 6, the algorithm is divided into two primary stages: *exploration* and *race-line following*; and comprises four core subsystems: *Hardware Interface*, *Navigation*, *Mission Control*, and *Visibility*. For inter-process coordination, we selected ROS 2 Foxy, given its broad sensor compatibility, robust documentation, and seamless integration with SLAM Toolbox and Nav2.

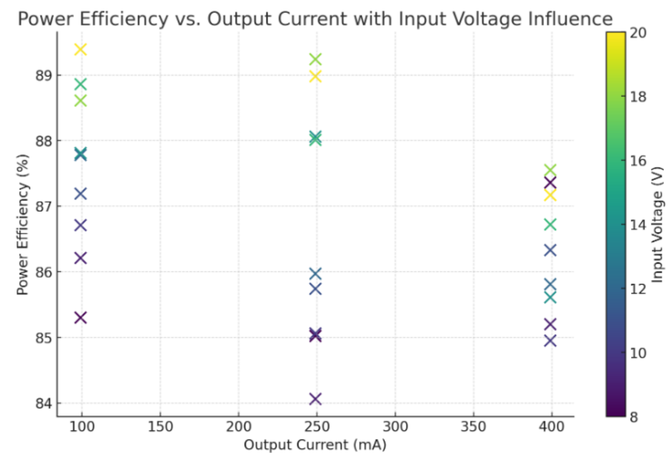

Fig. 5. Power efficiency of the 12 V regulators under varying load conditions.

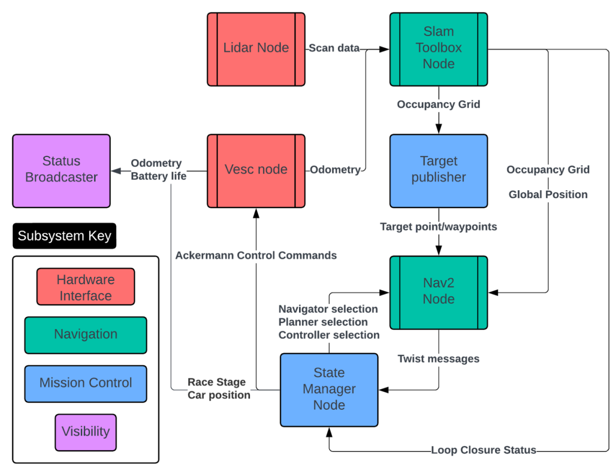

Fig. 6. High-level structure of the software subsystems.

A. Hardware Interface

The *Hardware Interface* subsystem issues commands to the motors and gathers data from the LiDAR and IMU sensors. We adopted the VESC interface provided by the RoboRacer foundation, which publishes odometry readings, and integrated ROS 2 drivers for the Hokuyo LiDAR to obtain standardized scan messages for subsequent processing.

B. Mission Control

Mission Control orchestrates the racing strategy via two ROS 2 nodes:

- **Target Publisher Node**: Determines the next pose(s) the vehicle must navigate toward.
- **State Manager Node**: Manages the race stage (exploration or race-line following) and adapts navigation outputs to the Hardware Interface. It acts as the overseeing force over the navigation subsystem built on top of Nav2.

Initially, the vehicle has no information about track geometry or its own global pose. The *exploration stage* addresses this limitation by incrementally mapping the environment and seeking uncharted regions until the track is fully mapped. During this stage, the Target Publisher Node receives continuous map updates from SLAM Toolbox, employs a breadth-first search to locate the most distant navigable cell, and forwards this goal to the Navigation subsystem. The State Manager Node converts the control commands from Navigation into a format acceptable to the Hardware Interface.

Once loop closure is detected, the State Manager Node sends a flag to both the Target Publisher Node and Navigation subsystem. The Target Publisher then calculates and publishes the race line, while the Navigation subsystem switches to plugins optimized for high-speed racing. Upon completing the race, the vehicle is halted via the connected console.

C. Navigation

The *Navigation* subsystem is composed of two key components: the SLAM Toolbox node and the Nav2 framework. SLAM Toolbox was selected due to its compatibility with Nav2 and its ability to perform loop closure detection, a critical feature for maintaining accurate maps over time. It receives sensor readings from hardware interface nodes, primarily LiDAR data, and constructs a pose graph to correctly position these readings relative to one another. This pose graph is then used to estimate the global position of the vehicle within the environment. SLAM Toolbox also generates an occupancy grid that represents both the vehicle's location and the positions of surrounding obstacles.

The Nav2 framework is responsible for planning and controlling the robot's motion. It is built around a set of ROS 2 action servers, each capable of managing a variety of plugins to handle specific tasks. In this setup, the most critical action servers are the Behavior Tree (BT) Navigator Server, the Planner Server, and the Controller Server.

- **BT Navigator Server**: Selects the appropriate plugin or behavior tree, e.g., `navigate_to_pose` or `navigate_through_poses`.
- **Planner Server**: Supports algorithms such as A* (for partial or unknown maps) and a lattice planner (optimized for smooth high-speed trajectories).
- **Controller Server**: Executes *pure pursuit* (slower, safer maneuvers) or *vector pursuit* (faster, continuous-curvature paths).

During the exploration phase, the BT Navigator repeatedly calls the A* planner and the *pure pursuit* controller, which is suitable for incomplete maps and conservative navigation (Fig. 7). This phase prioritizes caution and stability while gradually building an understanding of the environment. Once the race line is generated, the system transitions to a more aggressive mode of operation. The planning component switches to the Lattice planner, which generates smooth paths using a grid of splines that aim to follow the raceline as closely as possible while avoiding obstacles. This planner assigns costs to deviations from the raceline, ensuring that the chosen path maintains continuity and curvature, which is essential for high-speed navigation. Simultaneously, the controller switches to the *vector pursuit* plugin, which allows for faster, more responsive trajectory tracking. The combination of lattice-based planning and vector pursuit control ensures both precision and stability, reducing the likelihood of sharp steering inputs and enabling the vehicle to maintain speed safely while staying close to the optimal raceline.

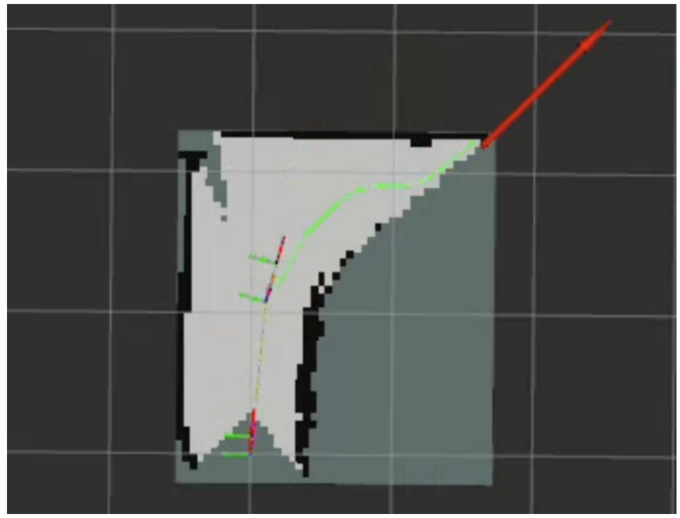

Fig. 7. Exploration phase workflow using A* and pure pursuit.

D. Visibility

The *Visibility* subsystem collects odometry and battery status from the Hardware Interface and monitors the vehicle's position and race stage from Mission Control. This information is transmitted over TCP to the Status Indicator Subsystem, enabling real-time user feedback. The Visibility node launches automatically at the start of each race and remains active until the race concludes.

VI. Status Indicator Subsystem

For real-time monitoring of the small-scale autonomous racing vehicle, an external subsystem was implemented to relay the vehicle's operational status to users during a race. This *Status Indicator Subsystem* enables quick access to vehicle diagnostics and serves as a mobile interface for remote status checks.

A. Hardware Design and Architecture

Fig. 8 illustrates the hardware configuration. A single cell 3.7 V LiPo battery powers the subsystem, allowing standalone operation without a constant wall-charger connection. Core components include:

- **ESP32 Microcontroller Unit (MCU)**: Manages communication with the vehicle via web sockets and drives the user interface.
- **4.0 in TFT Touchscreen Display**: Renders real-time data using the LVGL graphics library.
- **3.3 V / 5 V Regulator**: Conditions power from the LiPo battery and charging circuit, including a buck-boost converter for stable operation.

A 4.0-inch TFT touchscreen display was selected for the system primarily due to its lower power consumption compared to alternative display technologies. Table III outlines the current draw of the major components involved in the display subsystem.

TABLE III
POWER CONSUMPTION OF DISPLAY COMPONENTS

Component	Current Draw
LCD Panel	$\sim$10–20 mA
Backlight	$\sim$60–120 mA
Touch Controller (XPT2046)	$\sim$1–3 mA

To understand the total power profile of the system, Table IV summarizes the combined current draw of the ESP32 microcontroller and the touchscreen under various operational modes.

TABLE IV
COMBINED CURRENT DRAW OF ESP32 AND TOUCHSCREEN DISPLAY

Mode	Current Draw
Active (WiFi On)	$\sim$160–250 mA
Idle (WiFi Connected)	$\sim$40–80 mA
Deep Sleep	$\sim$10–150 μA

When the status indicator subsystem is fully active, the total combined current draw of the system is approximately 320mA. To ensure reliable operation and to accommodate transient current spikes or additional peripheral load, a power budget of 350–400mA is allocated. This buffer provides a safe margin for continuous and stable system performance.

The system is powered by a LiPo battery, which can be recharged using a USB charger board. During testing, the full recharge cycle takes approximately 30 minutes. Under normal operating conditions, the system draws around 320mA, with an additional 80mA of headroom reserved for overhead and peak loads. The theoretical runtime is calculated using the relationship:

$$\text{Runtime} = \frac{\text{Battery Capacity}}{\text{System Current}} = \frac{2500\,\text{mAh}}{400\,\text{mA}} \approx 6.25\,\text{hr}. \quad (8)$$

In practice, battery capacities vary between 2000mAh and 4000mAh, depending on the configuration. Accounting for real-world inefficiencies such as voltage drops, component tolerances, and thermal losses, the observed runtime typically ranges between 5 to 6 hours. This duration aligns well with the operational window of the racing vehicle and meets the demands of typical usage scenarios.

B. Functionality

The subsystem receives live updates from the racing vehicle's Jetson computing platform over a WebSocket connection, providing continuous telemetry on:

- **Vehicle Speed and Odometry**
- **Battery and Power Metrics**

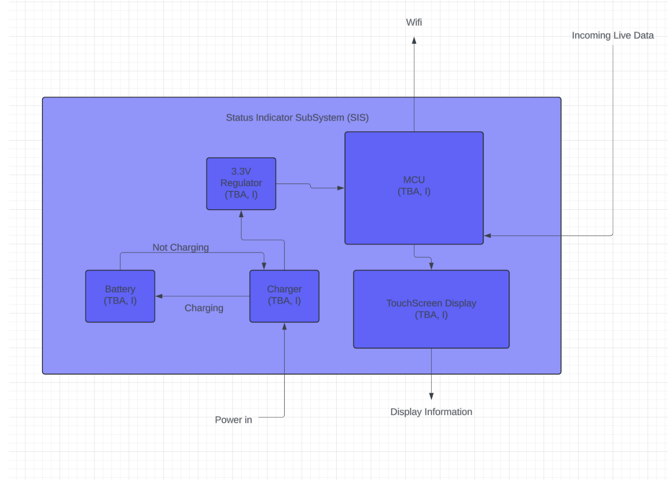

Fig. 8. Status Indicator Subsystem hardware and power flow.

- **Race Stage and System Status**

This data is displayed on the touchscreen via a user-friendly graphical interface. Operators can thus monitor the car's physical and computational state both short-term (during an ongoing race) and long-term (historical performance data). Overall, the Status Indicator Subsystem offers a portable, intuitive means to track vehicle behavior and optimize racing strategies in real time.

VII. CONCLUSION

This paper has presented the design and development of a small-scale autonomous racing vehicle platform, integrating mechanical, electrical, and software subsystems into a cohesive framework. The mechanical design focused on optimizing drivetrain performance, weight distribution, and suspension tuning, while a robust Power Management System efficiently supplied and monitored power for critical components. High-performance computing, based on the Jetson Xavier NX, enabled real-time perception and control, aided by LiDAR and depth camera sensors. The Status Indicator Subsystem further supported remote monitoring, allowing users to track vehicle status throughout a race.

A. Achievements

- **Robust Architecture:** A modular system architecture was implemented, combining power management, computing, and sensor fusion capabilities suitable for high-speed racing.
- **Mechanical Optimization:** Enhancements to the chassis, motor, and suspension improved acceleration, stability, and cornering performance, while maintaining a targeted 50/50 weight distribution (within $\pm 10\%$).
- **High Efficiency:** A custom-designed power board and voltage regulators consistently achieved over 60% efficiency, extending operational runtime and conserving battery resources.

- **Real-Time Autonomy:** ROS 2 Foxy and Nav2 facilitated SLAM-based navigation, path planning, and control strategies, enabling the vehicle to handle unknown racetracks with minimal intervention.
- **Comprehensive Monitoring:** The Status Indicator Subsystem provided real-time telemetry and diagnostics, improving user awareness and permitting immediate evaluations during testing or competition.

B. Impact and Application

The proposed solution offers a safe and cost-effective way to explore, develop, and validate cutting-edge self-driving algorithms at a smaller scale. By mirroring the core aspects of full-sized autonomous vehicles—such as AI-powered perception, mapping, and decision-making—this platform creates an accessible testbed for researchers and students. The technology aligns closely with real-world applications, including larger-scale autonomous vehicles, robotics research, and advanced driver-assistance systems (ADAS). Moreover, participation in competitions such as RoboRacer accelerates knowledge transfer and fosters innovation in the broader autonomous driving community.

C. Potential Improvements

Future work may target higher-level optimization and hardware refinements:

- **Expanded Sensor Suite:** Incorporating additional or more advanced sensors (e.g., radar, thermal cameras) could enhance robustness under diverse environmental conditions.
- **Enhanced Algorithms:** Machine learning or reinforcement learning components can supplement current classical approaches, potentially improving performance in dynamic racing scenarios.
- **Refined Power Management:** Further miniaturizing or fine-tuning the power system (e.g., adaptive power routing) could reduce weight while increasing energy efficiency.
- **Scalability:** Adaptations to handle higher speeds or larger vehicles would extend the utility of the platform, enabling more realistic or specialized test environments.

In summary, this small-scale racing platform demonstrates how precise mechanical design, efficient power management, advanced sensing, and robust software integration can combine to create a high-performance autonomous vehicle. The outcomes serve as a foundation for future research and development, bridging the gap between proof-of-concept prototypes and full-scale driverless systems.

Acknowledgment

This project was supported by the Connected and Autonomous Vehicle Research Lab (CAVREL), under the guidance of Dr. Yaser Fallah. The authors would like to extend their gratitude to the lab CAVREL for providing the necessary funding and resources that made this project possible. We also sincerely thank Dr. Arthur Weeks for his valuable assistance in helping us diagnosing and troubleshooting electrical design challenges encountered throughout the project.

Additionally, we express our deep appreciation to our reviewers and mentors for their insightful feedback and dedicated support. In particular, we would like to thank Dr. Yaser Fallah, Dr. Chinwendu Enyioha, Dr. Truong Nghiem, Dr. Hossein Magzoumi, Dr. Saleem Sahawneh, and Dr. ChungYong Chan, whose expertise and guidance enriched the development and execution of this work.

References

[1] RoboRacer Community, “Roboracer (f1tenth),” [Online]. Available: https://roboracer.ai

[2] RoboRacer Community, “24th Roboracer Autonomous Grand Prix,” [Online]. Available: https://icra2025-race.roboracer.ai/

[3] P. de Buck and J. R. R. A. Martins, “Minimum lap time trajectory optimization of performance vehicles with four-wheel drive and active aerodynamic control,” Vehicle System Dynamics, pp. 1–17, Jul. 2022. [Online]. Available: https://doi.org/10.1080/00423114.2022.2101930

[4] International Security Driver Association, “Weight Transfer - International Security Driver Association,” Mar. 24, 2013. [Online]. Available: https://isdacenter.org/weight-transfer/

[5] K. Parczewski and H. Wnek, “The influence of vehicle body roll angle on the motion stability and maneuverability of the vehicle,” Combustion Engines, vol. 168, no. 1, pp. 133–139, Feb. 2017. [Online]. Available: https://doi.org/10.19206/ce-2017-121